Eur. Phys. J. C 52, 425–434 (2007)
DOI 10.1140/epjc/s10052-007-0378-4

THE EUROPEAN PHYSICAL JOURNAL C

Regular Article – Theoretical Physics

# Plasmaneutrino spectrum

A. Odrzywołek[a]

M. Smoluchowski Institute of Physics, Jagiellonian University, Reymonta 4, 30-059 Krakow, Poland

Received: 10 April 2007 /
Published online: 11 August 2007 – 

**Abstract.** The spectrum of the neutrinos produced in the massive photon and longitudinal plasmon decay process has been computed with four levels of approximation for the dispersion relations. Some analytical formulae in the limit cases are derived. Interesting conclusions related to previous calculations of the energy loss in stars are presented. The high energy tail of the neutrino spectrum is shown to be proportional to $\exp(-E/kT)$, where $E$ is the neutrino energy and $kT$ is the temperature of the plasma.

**PACS.** 97.90.+j; 97.60.-s; 95.55.Vj; 52.27.Ep

## 1 Introduction and motivation

Thermal neutrino losses from a plasma are very important for stellar astrophysics [1,2]. Plasmon decay is one of the three main reactions. Extensive calculations for these processes were done by the group of Itoh [3–11]. Other influential articles include [12–20]. Meanwhile, our abilities to detect neutrinos has grown by many orders of magnitude, beginning with the 1.4 tonne experiment of Reines and Cowan [21] up to the biggest one existing now, the 50 kt super-Kamiokande detector [22]. Recently, the "GADZOOKS!" upgrade to Super-Kamiokande proposed by Beacom and Vagins [23] has attracted attention of both experimental and theoretical physicists. At least one new source of astrophysical antineutrinos is guaranteed with this upgrade, namely a diffuse supernova neutrino background [24–26]. Pre-supernova stars will be available to observations out to $\sim 2$ kps [26]. This technique is the only one extensible to the megaton scale [26]. Memphys, the Hyper-Kamiokande and UNO (for Mt-scale water Cherenkov detectors cf. e.g. [27]) proposals now seriously consider to add $GdCl_3$ to the one of the tanks with typically the three-tank design [28]. Recently, the discussion of geoneutrino detection [29] increased attention to deep underwater neutrino observatories [30] with a target mass of 5–10 Mt [26] and even larger [31]. It seems that (anti-) neutrino astronomy is on our doorstep, but numerous astrophysical sources of the $\nu$ still are not analyzed from the detection point of view.

Detection of the solar [32–40] and supernova [41–49] neutrinos was accompanied and followed by an extensive set of detailed calculations (see e.g. [50–57] and references therein as representatives of this broad subject) of the neutrino spectrum. On the contrary, very little is known about spectral neutrino emission from other astrophysical objects. Usually, some analytical representation of the spectrum is used, based on earlier experience and numerical simulations; cf. e.g. [58]. While this approach is justified for supernovae, where neutrinos are trapped, other astrophysical objects are transparent to neutrinos, and the spectrum can be computed with arbitrary precision. Our goal is to compute neutrino spectra as exact as possible and fill this gap. The plasmaneutrino process dominates dense, degenerate objects like red giant cores [59], cooling white dwarfs [60], including Ia supernova progenitors before the so-called "smoldering" phase [61]. Plasmaneutrino is important secondary cooling processes in neutron star crusts [62] and massive stars [63]. Unfortunately, thermal neutrino losses usually are calculated using methods completely erasing almost any information related to the neutrino energy $\mathcal{E}_\nu$ and the directionality as well. This information is not required to compute the total energy $Q$ radiated as neutrinos per unit volume and time. From the experimental point of view, however, it is extremely important if a given amount of energy is radiated as e.g. numerous keV neutrinos or one 10 MeV neutrino. In the first case we are unable to detect (using available techniques) any transient neutrino source regardless of the total luminosity and proximity of the object. In the second case we can detect astrophysical neutrino sources if they are strong and not too far away using an advanced detector that is big enough.

A few of the research articles in this area attempt to estimate the average neutrino energy [16,17,65,66], additionally computing the reaction rate $R$. Strangely, the authors of these references presented figures and formulae for $Q/R$ instead of $\frac{1}{2}Q/R$. This gives a false picture of the real situation, as the former expression gives $\langle \mathcal{E}_\nu + \mathcal{E}_{\bar{\nu}} \rangle$. Obviously, we detect *neutrinos*, not $\nu$–$\bar{\nu}$ pairs. Values of $\frac{1}{2}Q/R$ *do not* give the average neutrino energy, as in gen-

[a] e-mail: odrzywolek@th.if.uj.edu.pl

eral the neutrino and antineutrino spectra are different. As we will see, *only* for longitudinal plasmon decay neutrinos the energies of neutrinos and antineutrinos are equal. However, the difference in all situations where thermal neutrino losses are important is numerically small and the formula

$$\langle \mathcal{E}_\nu \rangle \simeq \frac{1}{2}\frac{Q}{R} \tag{1}$$

is still a "working" estimate.

The mean neutrino energy is useful for the purpose of a qualitative discussion of the detection prospects/methods. A quantitative discussion requires knowledge of the spectrum shape (the differential emissivity $\mathrm{d}R/\mathrm{d}\mathcal{E}_\nu$). The high energy tail is particularly important from the point of view of experimental detection. Detection of the lowest energy neutrinos is extremely challenging due to numerous background signal noise sources e.g. $^{14}$C decay for $\mathcal{E}_\nu < 200\,\mathrm{keV}$ [64]. Relevant calculations for the spectrum of the medium energy neutrinos with $\langle \mathcal{E}_\nu \rangle \sim 1\,\mathrm{MeV}$ emitted from thermal processes have become available recently [65–67]. The purpose of this article is to develop accurate methods and discuss various theoretical and practical (important for detection) aspects of the spectra of neutrinos from astrophysical plasma processes. This could help experimental physicists to discuss a possible realistic approach to detect astrophysical sources of neutrinos in the future.

## 2 Plasmaneutrino spectrum

### 2.1 Properties of plasmons

Emissivity and the spectrum shape from plasmon decay is strongly affected by the dispersion relation for transverse plasmons (massive in-medium photons) and longitudinal plasmons. In contrast to transverse plasmons, with the vacuum dispersion relation $\omega(k) = k$, longitudinal plasmons exist only in the plasma. The dispersion relation by definition is a function $\omega(k)$, where $\hbar\omega$ is the energy of the (quasi-) particle and $\hbar k$ is the momentum. The issues related to particular handling of these functions are discussed clearly in the article of Braaten–Segel [15]. We will repeat here the most important features of the plasmons.

For both types, the plasmon energy for momentum $k = 0$ is equal to $\omega_0$. The value $\omega_0 \equiv \omega(0)$ is referred to as the *plasma frequency* and can be computed from

$$\omega_0^2 = \frac{4\alpha}{\pi}\int_0^\infty \frac{p^2}{E}\left(1 - \frac{v^2}{3}\right)(f_1 + f_2)\,\mathrm{d}p\,, \tag{2}$$

where $v = p/E$ and $E = \sqrt{p^2 + m_e^2}$ ($\hbar = c = 1$ units are used), $m_e \simeq 0.511\,\mathrm{MeV}$, and the fine structure constant is $\alpha = 1/137.036$ [68]. The functions $f_1$ and $f_2$ are the Fermi–Dirac distributions for electrons and positrons, respectively:

$$f_1 = \frac{1}{\mathrm{e}^{(E-\mu)/kT} + 1}\,, \quad f_2 = \frac{1}{\mathrm{e}^{(E+\mu)/kT} + 1}\,. \tag{3}$$

The quantity $\mu$ is the chemical potential of the electron (including the rest mass). Other important parameters include the first relativistic correction $\omega_1$,

$$\omega_1^2 = \frac{4\alpha}{\pi}\int_0^\infty \frac{p^2}{E}\left(\frac{5}{3}v^2 - v^4\right)(f_1 + f_2)\,\mathrm{d}p\,, \tag{4}$$

the maximum longitudinal plasmon momentum (energy) $k_{\max}$,

$$k_{\max}^2 \equiv \omega_{\max}^2 = \frac{4\alpha}{\pi}\int_0^\infty \frac{p^2}{E}\left(\frac{1}{v}\ln\frac{1-v}{1+v} - 1\right)(f_1 + f_2)\,\mathrm{d}p\,, \tag{5}$$

and the asymptotic transverse plasmon mass $m_\mathrm{t}$,

$$m_\mathrm{t}^2 = \frac{4\alpha}{\pi}\int_0^\infty \frac{p^2}{E}(f_1 + f_2)\,\mathrm{d}p\,. \tag{6}$$

The quantity $m_\mathrm{t}$ is often referred to as the thermal photon mass. We also define the parameter $v_*$:

$$v_* = \frac{\omega_1}{\omega_0} \tag{7}$$

interpreted as the typical velocity of the electrons in the plasma [15]. The axial polarization coefficient is

$$\omega_\mathrm{A} = \frac{2\alpha}{\pi}\int_0^\infty \frac{p^2}{E^2}\left(1 - \frac{2}{3}v^2\right)(f_1 - f_2)\,\mathrm{d}p\,. \tag{8}$$

The value of $\omega_\mathrm{A}$ is a measure of the difference between the neutrino and antineutrino spectra. The set of numerical values used to display this sample result is presented in Table 1.

The values of $\omega_0, \omega_{\max}, m_\mathrm{t}$ define a sub-area of the $\omega$–$k$ plane, where the dispersion relations for the photons $\omega_\mathrm{t}(k)$ and the longitudinal plasmons $\omega_\mathrm{l}(k)$ are found:

$$\max(k, \omega_0) \le \omega_\mathrm{l}(k) \le \omega_{\max}, \quad 0 \le k \le k_{\max}\,, \tag{9a}$$

$$\sqrt{k^2 + \omega_0^2} \le \omega_\mathrm{t}(k) \le \sqrt{k^2 + m_\mathrm{t}^2}, \qquad 0 \le k \le \infty\,. \tag{9b}$$

The dispersion relations are solutions to the equations [15]

$$k^2 = \Pi_\mathrm{l}\left(\omega_\mathrm{l}(k), k\right) \tag{10a}$$

$$k^2 = \omega_\mathrm{t}(k)^2 - \Pi_\mathrm{t}\left(\omega_\mathrm{t}(k), k\right)\,, \tag{10b}$$

**Table 1.** Plasma properties for a typical massive star during Si burning. All values are in MeV

| $kT$ | $\mu$ | $\omega_0$ | $\omega_1$ | $m_\mathrm{t}$ | $\omega_{\max}$ | $\omega_\mathrm{A}$ |
|---|---|---|---|---|---|---|
| 0.32 | 1.33 | 0.074 | 0.070 | 0.086 | 0.133 | 0.002 |

where the longitudinal and transverse polarization functions are given as integrals:

$$\Pi_{\rm l} = \frac{4\alpha}{\pi}\int\limits_0^\infty \frac{p^2}{E}\left(\frac{\omega_{\rm l}}{vk}\ln\frac{\omega_{\rm l}+vk}{\omega_{\rm l}-vk} - 1 - \frac{\omega_{\rm l}^2-k^2}{\omega_{\rm l}^2-v^2k^2}\right) \times (f_1+f_2)\,{\rm d}p\,, \tag{11a}$$

$$\Pi_{\rm t} = \frac{4\alpha}{\pi}\int\limits_0^\infty \frac{p^2}{E}\left(\frac{\omega_{\rm t}^2}{k^2} - \frac{\omega_{\rm t}^2-k^2}{k^2}\frac{\omega_{\rm t}}{2vk}\ln\frac{\omega_{\rm t}+vk}{\omega_{\rm t}-vk}\right) \times (f_1+f_2)\,{\rm d}p\,. \tag{11b}$$

A typical example of the exact plasmon dispersion relations is presented in Fig. 1 (see the dash-dotted curve). As solving (10a) and (10b) with (11) is computationally intensive, three levels of approximation for the dispersion relations are widely used:

1. zero-order analytical approximations;
2. first-order relativistic corrections;
3. the Braaten–Segel approximation.

### 2.1.1 Approximations for longitudinal plasmons

For longitudinal plasmons, the simplest zero-order approach used in the early calculations of Adams et al. [13] and more recently in [66] for the photoneutrino process is to put simply

$$\omega(k) = \omega_0\,, \tag{12}$$

where $\omega_0$ is the plasma frequency (2). The maximum plasmon energy is $\omega_{\rm max} = \omega_0$ in this approximation. The zero-order approximation is valid only for the non-relativistic regime and leads to large errors of the total emissivity [12].

The first relativistic correction to (12) has been introduced by Beaudet et al. [12]. The dispersion relation $\omega_{\rm l}(k)$ is given in an implicit form:

$$\omega_{\rm l}^2 = \omega_0^2 + \frac{3}{5}\omega_{\rm l}^2\frac{k^2}{\omega_{\rm l}^2}\,, \tag{13}$$

with the maximum plasmon energy equal to

$$\omega_{\rm max}^{(1)} = \sqrt{\omega_0^2 + \frac{3}{5}\omega_{\rm l}^2}\,. \tag{14}$$

This approximation, however, does not introduce a really serious improvement (see Figs. 1, 2 (left) and 4). A breaking point was the publication of the Braaten–Segel approximation [15]. Using the simple analytical equation

$$k^2 = 3\frac{\omega_0^2}{v_*^2}\left(\frac{\omega_{\rm l}}{2v_*k}\ln\frac{\omega_{\rm l}+v_*k}{\omega_{\rm l}-v_*k} - 1\right)\,, \tag{15}$$

where $v_*$ is defined in (7), one is able to get an almost exact dispersion relation; cf. Figs. 1 and 2, left panels. The solution to (15) exists in the range $1 < k < k_{\rm max}^{\rm BS}$, where, in this approximation, the maximum longitudinal plasmon momentum is

$$\left(\omega_{\rm max}^{\rm BS}\right)^2 = \frac{3\omega_0^2}{2v_*^2}\left(\frac{1}{2v_*}\ln\frac{1+v_*}{1-v_*} - 1\right)\,, \tag{16}$$

which gives a value slightly different from the exact value (Fig. 2, left), but it is required for consistency of the approximation.

### 2.1.2 Approximations for transverse plasmons

For photons in vacuum the dispersion relation is $\omega_{\rm t} = k$. The zero-order approximation for in-medium photons is

$$\omega_{\rm t}^2 = \omega_0^2 + k^2, \quad k \ll \omega_0\,, \tag{17a}$$

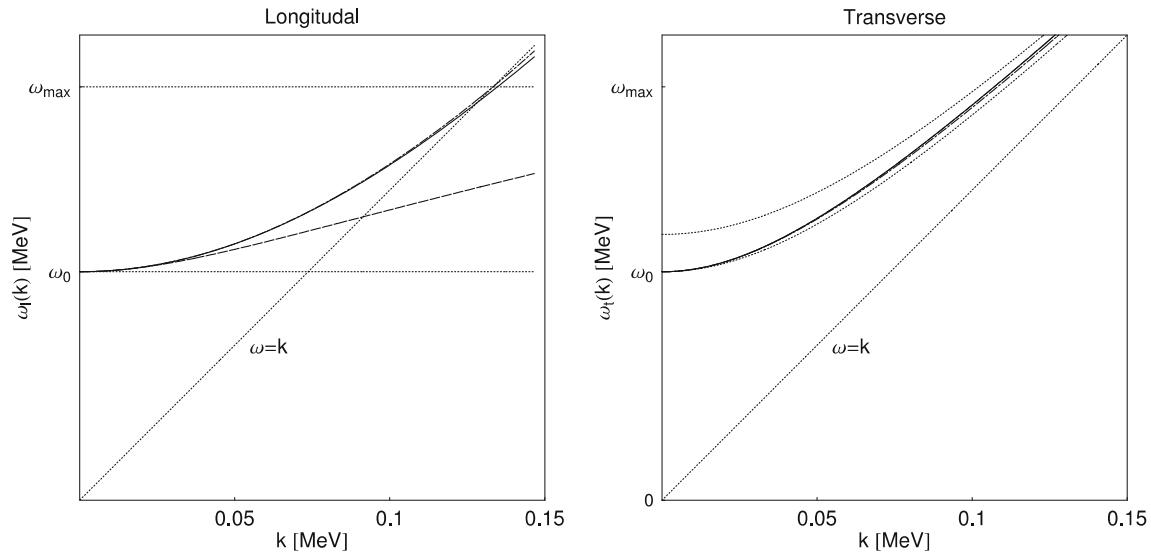


**Fig. 1.** Longitudinal and transverse plasmon dispersion relation $\omega_{\rm l,t}(k)$ for the plasma parameters from Table 1. The exact result (*dot-dashed*) is very close to the Braaten–Segel approximation (*solid*). Zero-order (*dotted*) and first-order (*dashed*) approximations are very poor, especially for the londitudinal mode (*left*)

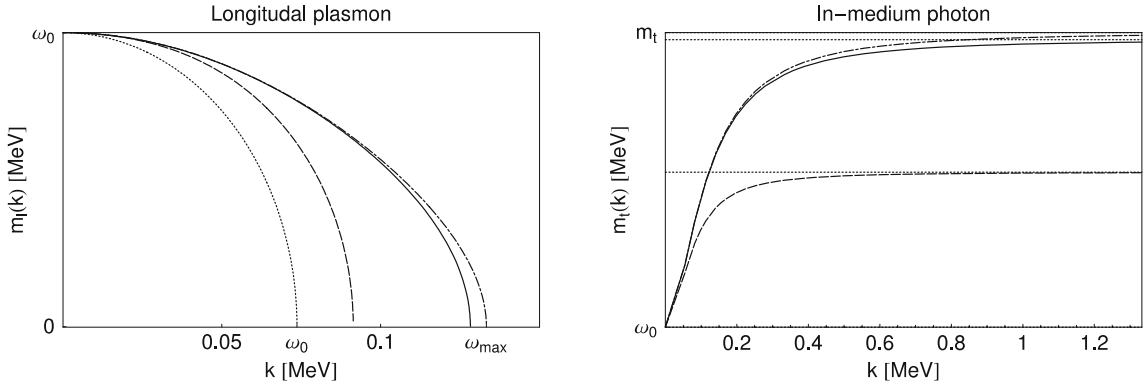


**Fig. 2.** Longitudinal and transverse plasmon mass. *Dotted lines* on the *right panel* show the asymptotic transverse mass. *Line dashing* is the same as in Fig. 1

valid for small $k$, and

$$\omega_{\mathrm{t}}^2 = m_{\mathrm{t}}^2 + k^2, \quad k \gg \omega_0\,, \tag{17b}$$

valid for very large $k$. Formulae (17a) and (17b) provide lower and upper limits for a realistic $\omega_{\mathrm{t}}(k)$, respectively (cf. Fig. 1, right panel, dotted curve). First-order relativistic corrections lead to the formula

$$\omega_{\mathrm{t}}^2 = \omega_0^2 + k^2 + \frac{1}{5}\omega_1^2\frac{k^2}{\omega_{\mathrm{t}}^2}\,, \tag{18}$$

with the asymptotic photon mass

$$m_{\mathrm{t}}^{(1)} = \sqrt{\omega_0^2 + \omega_1^2/5}\,. \tag{19}$$

Finally, the Braaten–Segel approximation leads to

$$\omega_{\mathrm{t}}^2 = k^2 + \omega_0^2\frac{3\omega_{\mathrm{t}}^2}{2v_*^2k^2}\left(1 - \frac{\omega_{\mathrm{t}}^2 - v_*^2k^2}{2\omega_{\mathrm{t}}v_*k}\ln\frac{\omega_{\mathrm{t}} + v_*k}{\omega_{\mathrm{t}} - v_*k}\right). \tag{20}$$

The asymptotic photon mass $m_{\mathrm{t}}^{\mathrm{BS}}$ derived from (20) is

$$\left(m_{\mathrm{t}}^{\mathrm{BS}}\right)^2 = \frac{3\omega_0^2}{2v_*^2}\left(1 - \frac{1-v_*^2}{2v_*}\ln\frac{1+v_*}{1-v_*}\right). \tag{21}$$

This is slightly smaller (left panel of Fig. 2, dashed curve) than the exact value (solid line).

All four relations are presented in Fig. 1. Differences are clearly visible, but they are much less pronounced for transverse than for longitudinal plasmons. Inspection of Fig. 2 reveals, however, that in the large momentum regime the asymptotic behavior is correct only for the exact integral relations (10b) and may be easily reproduced using (17b) with $m_{\mathrm{t}}$ from (6).

Let us recapitulate the main conclusions. The Braaten–Segel approximation provides a reasonable approximation, as the nonlinear equations (15) and (20) are easily solved using e.g. the bisection method. The zero- and first-order approximations (12), (17a) and (17b) with the limit values (9) provide the starting points and ranges. The approximation has been tested by [69] and is considered as the best one available [20]. Errors for the part of the $kT$–$\mu$ plane where the plasmaneutrino process *is not dominant* may be as large as 5% [69]. At present, these inaccuracies are irrelevant for any practical application, and the Braaten–Segel approximation is recommended for all purposes.

## 2.2 Plasmon decay rate

In the standard model of the electroweak interactions, massive in-medium photons and longitudinal plasmons may decay into neutrino–antineutrino pairs:

$$\gamma^* \to \nu_x + \bar{\nu}_x. \tag{22}$$

In the first-order calculations two Feynman diagrams (see Fig. 3) contribute to the decay rate [15, 65].

For the decay of the longitudinal plasmon the squared matrix element is

$$M_{\mathrm{l}}^2 = \frac{G_{\mathrm{F}}^2C_{\mathrm{V}}^2}{\pi\alpha}\left(\omega_{\mathrm{l}}^2 - k^2\right)^2\left[\frac{2K\cdot Q_1K\cdot Q_2}{K^2} + \frac{2\mathbf{k}\cdot\mathbf{q}_1\mathbf{k}\cdot\mathbf{q}_2}{k^2} - Q_1\cdot Q_2\right], \tag{23a}$$

where $K = (\omega, \mathbf{k})$ is the four-momentum of the plasmon. $Q_1 = (\mathcal{E}_1, \mathbf{q}_1)$ and $Q_2 = (\mathcal{E}_2, \mathbf{q}_2)$ are the four-momentum of the neutrino and antineutrino, respectively.

The squared matrix element for decay of the massive photon is

$$M_{\mathrm{t}}^2 = \frac{G_{\mathrm{F}}^2}{\pi\alpha}\left[\left(C_{\mathrm{V}}^2\Pi_{\mathrm{t}}^2 + C_{\mathrm{A}}^2\Pi_{\mathrm{A}}^2\right)\left(\mathcal{E}_1\mathcal{E}_2 - \frac{\mathbf{k}\cdot\mathbf{q}_1\mathbf{k}\cdot\mathbf{q}_2}{k^2}\right) + 2C_{\mathrm{V}}C_{\mathrm{A}}\Pi_{\mathrm{t}}\Pi_{\mathrm{A}}\frac{\mathcal{E}_1\mathbf{k}\cdot\mathbf{q}_2 - \mathcal{E}_2\mathbf{k}\cdot\mathbf{q}_1}{k}\right], \tag{23b}$$

where $\Pi_{\mathrm{t}}$ is defined in (11b) and the axial polarization function $\Pi_{\mathrm{A}}$ reads

$$\Pi_{\mathrm{A}} = \frac{2\alpha}{\pi}\frac{\omega_{\mathrm{t}}^2 - k^2}{k}\int_0^\infty\frac{p^2}{E^2}\left(\frac{\omega_{\mathrm{t}}}{2vk}\ln\frac{\omega_{\mathrm{t}} + vk}{\omega_{\mathrm{t}} - vk} - \frac{\omega_{\mathrm{t}}^2 - k^2}{\omega_{\mathrm{t}}^2 - v^2k^2}\right)\times(f_1 - f_2)\,\mathrm{d}p\,. \tag{24}$$

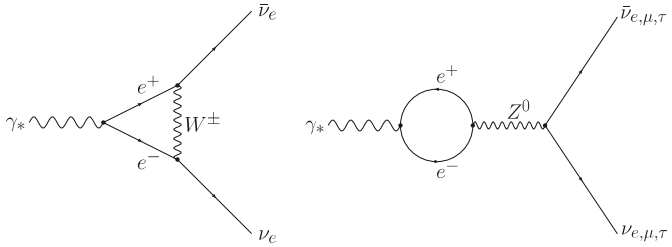


**Fig. 3.** Feynman diagrams for plasmon decay

The Fermi constant is $G_\mathrm{F}/(\hbar c)^3 = 1.16637(1)\ 10^{-5}\,\mathrm{GeV}^{-2}$ [68] and, in the standard model of the electroweak interactions, the vector and axial coupling constants are

$$C_\mathrm{V}^e = \frac{1}{2} + 2\sin^2\theta_\mathrm{W}\,, \quad C_\mathrm{A}^e = \frac{1}{2} \tag{25}$$

$$C_\mathrm{V}^{\mu,\tau} = -\frac{1}{2} + 2\sin^2\theta_\mathrm{W}\,, \quad C_\mathrm{A}^{\mu,\tau} = -\frac{1}{2} \tag{26}$$

for electron and $\mu,\tau$ neutrinos, respectively. The Weinberg angle is $\sin^2\theta_\mathrm{W} = 0.23122(15)$ [68].

Terms containing $C_\mathrm{A}$ (the so-called axial contribution) in (23b) are frequently treated separately [65] or removed at all [3]. In calculations concentrated on the total emissivity this is justified as antisymmetric terms multiplied by $C_\mathrm{V}C_\mathrm{A}$ do not contribute at all and terms $C_\mathrm{A}^2 \times \ldots$ are suppressed relative to the term beginning with $C_\mathrm{V}^2 \times \ldots$ by four orders of magnitude [3]. However, if one attempts to compute the neutrino energy spectrum all three terms should be added, as the mixed V–A "channel" alone leads to a negative emission probability for some neutrino energy range (Fig. 6), which is physically unacceptable. These terms remain numerically small but *only* for electron neutrinos. For $\mu$ and $\tau$ neutrino spectra the *axial* part contributes at $\sim 1\%$ level due to the very small value $C_\mathrm{V}^{\mu,\tau} = -0.0376$, while still $C_\mathrm{A} = -0.5$. The 'mixed' term leads to significant differences between the $\nu_{\mu,\tau}$ and $\bar{\nu}_{\mu,\tau}$ spectra; cf. Fig. 6. Relative contributions of the three transverse "channels" for electron and $\mu,\tau$ are presented in Table 2.

In general, all the terms in the squared matrix element (23b) should be added. We have only *two* different spectra: the longitudinal and the transverse one.

The particle production rate from plasma in thermal equilibrium is

$$R_i = \frac{g_i}{(2\pi)^5} \times \int Z_i f_{\gamma^*} \delta^4(K - Q_1 - Q_2) M_i^2 \frac{\mathrm{d}^3\mathbf{k}}{2\omega_i} \frac{\mathrm{d}^3\mathbf{q}_1}{2\mathcal{E}_1} \frac{\mathrm{d}^3\mathbf{q}_2}{2\mathcal{E}_2}\,, \tag{27}$$

where $i = \mathrm{l}$ for the longitudinal mode and $i = \mathrm{t}$ for the transverse mode. The Bose–Einstein distribution for plasmons $f_{\gamma^*}$ is

$$f_{\gamma^*} = \frac{1}{\mathrm{e}^{\omega_{\mathrm{t,l}}/kT} - 1}\,, \tag{28}$$

**Table 2.** Relative weight of the $M_\mathrm{t}^2$, see (23b), terms for $e$ and $\mu,\tau$ neutrinos

| Flavor | Vector $\frac{C_V^2\omega_0^4}{(C_V\omega_0^2+C_\mathrm{A}\omega_\mathrm{A})^2}$ | Axial $\frac{C_\mathrm{A}^2\omega_\mathrm{A}^2}{(C_V\omega_0^2+C_\mathrm{A}\omega_\mathrm{A})^2}$ | Mixed $\frac{2C_VC_\mathrm{A}\omega_0^2\omega_\mathrm{A}}{(C_V\omega_0^2+C_\mathrm{A}\omega_\mathrm{A})^2}$ |
|---|---|---|---|
| electron | 0.74 | 0.02 | 0.24 |
| mu/tau | 0.07 | 0.39 | 0.54 |

and the residue factors $Z_{\mathrm{t,l}}$ are expressed by the polarization functions $\Pi_{\mathrm{t,l}}$ of (11b) and (11a):

$$Z_\mathrm{t}^{-1} = 1 - \frac{\partial\Pi_\mathrm{t}}{\partial\omega^2} \tag{29}$$

$$Z_\mathrm{l}^{-1} = -\frac{\omega_\mathrm{l}^2}{k^2}\frac{\partial\Pi_\mathrm{l}}{\omega^2}. \tag{30}$$

For massive photons $g_\mathrm{t} = 2$ and for the longitudinal plasmon $g_\mathrm{l} = 1$.

The differential rates[1] were derived for the first time in [65]. Here, we present the result in the form valid for both types of plasmons, ready for calculations using any available form of dispersion relation:

$$\frac{\mathrm{d}^2R_i}{\mathrm{d}\mathcal{E}_1\,\mathrm{d}\mathcal{E}_2} = \frac{g_i}{\pi^4} Z_i M_i^2 f_{\gamma^*} J_i \mathcal{S}\,, \tag{31}$$

where $i = \mathrm{l}$ or $i = \mathrm{t}$. The product $\mathcal{S}$ of the unit step functions $\Theta$ in (31) restrict the result to the kinematically allowed area:

$$\mathcal{S} = \Theta(4\mathcal{E}_1\mathcal{E}_2 - m_i^2)\Theta(\mathcal{E}_1 + \mathcal{E}_2 - \omega_0)\Theta(\omega_\mathrm{max} - \mathcal{E}_1 - \mathcal{E}_2)\,. \tag{32}$$

The four-momenta in the squared matrix element are

$$\begin{aligned} Q_1 &= (\mathcal{E}_1, 0, 0, \mathcal{E}_1)\,,\\ Q_1 &= (\mathcal{E}_2, \mathcal{E}_2\sin\theta, 0, \mathcal{E}_2\cos\theta)\,,\\ K &= (\mathcal{E}_1 + \mathcal{E}_2, \mathcal{E}_2\sin\theta, 0, \mathcal{E}_1 + \mathcal{E}_2\cos\theta)\,,\\ m_i^2 &= KK = (\mathcal{E}_1 + \mathcal{E}_2)^2 - k'^2\,,\\ \cos\theta &= \frac{k'^2 - \mathcal{E}_1^2 - \mathcal{E}_2^2}{2\mathcal{E}_1\mathcal{E}_2}\,,\\ k' &= \omega_{\mathrm{l,t}}^{-1}(\mathcal{E}_1 + \mathcal{E}_2)\,,\\ \omega_i &= \mathcal{E}_1 + \mathcal{E}_2\,, \end{aligned}$$

where $\omega_i^{-1}$ denotes the function *inverse* to the dispersion relation. The Jacobian $J_i$ arising from the Dirac delta integration in (27) is

$$J_i^{-1} = \frac{\mathcal{E}_1\mathcal{E}_2}{k'}\left.\frac{\partial\omega_i}{\partial k}\right|_{k=k'}. \tag{33}$$

[1] The double differential rate $\mathrm{d}^2R_i/\,\mathrm{d}\mathcal{E}\,\mathrm{d}\cos\theta$ has an identical form as (31), but now four-momenta cannot be given explicitly, unless a simple analytical approximation for $\omega_i(k)$ is used. Analytical approximations for the spectrum shape are derived this way.

The residue factors $Z_i$ are given in (30) and (29). The maximum energy $\omega_{\max}$ in (32) for longitudinal plasmons must be in agreement with the particular approximation used for $\omega_{\mathrm{l}}(k)$: $\omega_0$, (14) or (16) for the zero-order equation (12), and first-order, (13) or the Braaten–Segel equation (15), respectively. For transverse plasmons $\omega_{\max} \to \infty$, and the last $\Theta$ function in (32) has no effect and may be omitted.

## 2.3 Longitudinal neutrino spectrum

### 2.3.1 Analytical approximation

We begin with a general remark on the spectrum. Note that (31) is symmetric for a longitudinal mode under the change $\mathcal{E}_{1,2} \to \mathcal{E}_{2,1}$, because (23a) is symmetric with respect to the exchange $Q_{1,2} \to Q_{2,1}$. The resulting energy spectrum is thus identical for neutrinos and antineutrinos. This is not true for transverse plasmons with the axial contribution included; cf. Sect. 2.4.

Using the zero-order dispersion relation for longitudinal plasmons, (12), we are able to express the spectrum by elementary functions. The longitudinal residue factor $Z_{\mathrm{t}}$ is now

$$Z_{\mathrm{l}}^0 = 1\,, \tag{34}$$

and the Jacobian $J_{\mathrm{l}}$ resulting from the integration of the Dirac delta function is

$$J_{\mathrm{l}}^0 = 1\,. \tag{35}$$

Now, the differential rate $\mathrm{d}^2R/\,\mathrm{d}\mathcal{E}\,\mathrm{d}\cos\theta$ (cf. (31) and footnote 1) becomes much simpler, and the integral over $\mathrm{d}\cos\theta$ can be evaluated analytically. Finally, we get the longitudinal spectrum,

$$\frac{\mathrm{d}R}{\mathrm{d}\mathcal{E}} \equiv \lambda(\mathcal{E}) = \frac{{G_{\mathrm{F}}}^2 {C_{\mathrm{V}}}^2 {\omega_0}^7}{1260\pi^4\alpha\hbar^3c^9} \frac{f(\mathcal{E}/\omega_0)}{\mathrm{e}^{\omega_0/kT}-1}\,, \tag{36}$$

where the normalized spectrum is

$$f(x) = \frac{105}{32}\left[4x(x-1)(8x^4-16x^3+2x^2+6x-3) + 3(1-2x)^2\ln(1-2x)^2\right]. \tag{37}$$

Let us note that $f$ is undefined at $x = 1/2$; we use the limit

$$\lim_{x\to 1/2} f(x) = 105/32$$

instead. The function $f(x)$ is symmetric with respect to the point $x = 1/2$, where $f$ has a maximum value (see Fig. 4, dotted line).

In this limit, correct for a non-relativistic, non-degenerate plasma, the average neutrino and antineutrino energy is $\langle\mathcal{E}\rangle = \omega_0/2$, and the maximum $\nu$ energy is $\omega_0$.

Inspection of Fig. 4 reveals little difference between the analytical result (36) and the result obtained with first-order relativistic corrections to the dispersion relation (13).

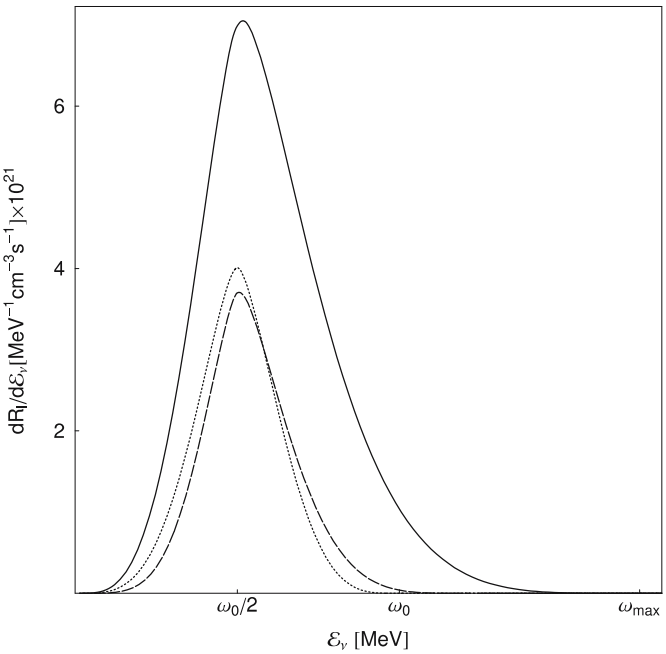


**Fig. 4.** Approximate longitudinal plasmon analytical neutrino spectrum, see (36), (*dotted*), with first-order correction used by BPS [12] (*dashed*), and spectrum computed using the dispersion relation [15] (*solid*). Plasma properties are according to Table 1

### 2.3.2 Numerical results

The simple formula (36) significantly underestimates the flux and the maximum neutrino energy, equal to $\omega_{\max}$ rather than $\omega_0$. Therefore, we have used the Braaten–Segel approximation for the longitudinal plasmon dispersion relation.

To derive the spectrum we will use the form of the differential rate (31) provided by [65]. In the Braaten–Segel approximation we have

$$Z_{\mathrm{l}}^{\mathrm{BS}} = \frac{\omega_{\mathrm{l}}^2}{\omega_{\mathrm{l}}^2-k^2}\frac{2(\omega_{\mathrm{l}}^2-v_*^2k^2)}{3\omega_0^2-\omega_{\mathrm{l}}^2+v_*^2k^2}\,,$$
$$J_{\mathrm{l}}^{\mathrm{BS}} = \left|\frac{k^2}{\mathcal{E}_1\mathcal{E}_2}\frac{1-\beta_{\mathrm{l}}}{\omega_{\mathrm{l}}\beta_{\mathrm{l}}}\right|,$$
$$\beta_{\mathrm{l}}^{\mathrm{BS}} = \frac{3\omega_0^2}{2v_*^3}\left(\frac{3\omega_{\mathrm{l}}}{2k^3}\ln\frac{\omega_{\mathrm{l}}+v_*k}{\omega_{\mathrm{l}}-v_*k} - \frac{\omega_{\mathrm{l}}^2v_*}{k^2(\omega_{\mathrm{l}}^2-v_*^2k^2)} - \frac{2v_*}{k^2}\right).$$

The spectrum is computed as an integral of (31) over $\mathrm{d}\mathcal{E}_2$. An example is presented in Fig. 4. Integration of the function in Fig. 4 over the neutrino energy gives a result well in agreement with both (30) from [15] and (54) from [65].

## 2.4 Transverse plasmon decay spectrum

### 2.4.1 Analytical approximation

The derivation of the massive in-medium photon decay spectrum closely follows the previous subsection. Semi-analytical formula can be derived for the dispersion rela-

tions (17). For the dispersion relation (17b) the transverse residue factor $Z_{\rm t}$ is

$$Z_{\rm t}^0 = 1\,, \tag{38}$$

the polarization function $\Pi_{\rm t}$ is equal to

$$\Pi_{\rm t}^0 = m_{\rm t}^2\,, \tag{39}$$

and the Jacobian resulting from integration of the Dirac delta function $J_{\rm t}$ is

$$J_{\rm t}^0 = \frac{\mathcal{E}_1 + \mathcal{E}_2}{\mathcal{E}_1 \mathcal{E}_2}\,. \tag{40}$$

The approximate spectrum, neglecting differences between neutrinos and antineutrinos, is given by the following integral:

$$\lambda(\mathcal{E}) = \frac{G_{\rm F}^2 C_{\rm V}^2}{64\pi^4\alpha}\frac{m_{\rm t}^7}{\hbar^3 c^9}\int\limits_{-1}^{1}\frac{P(\cos\theta, \mathcal{E}/m_{\rm t})\,{\rm d}\cos\theta}{\exp\left[(\mathcal{E}+\frac{m_{\rm t}^2}{2\mathcal{E}(1-\cos\theta)})/kT\right]-1}\,, \tag{41}$$

where the rational function $P(ct, x)$ is

$$P(ct,x) = \frac{1+2(ct-1)^2(2x^2-1)x^2}{x(ct-1)^2[1-2ct(ct-1)x^2+2(ct-1)^2)x^4]}\,. \tag{42}$$

The result presented in Fig. 7 shows that the spectrum (41) obtained with the dispersion relation (17b) agrees well

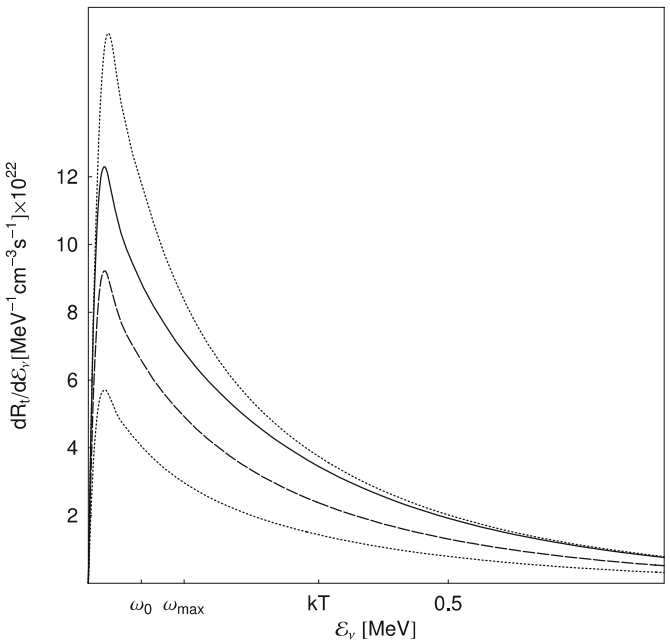


**Fig. 5.** Transverse plasmaneutrino spectrum computed from the approximation [15] (*solid*) with upper and lower limits, (17b) and (17a), for the dispersion relation (*dotted*). The first-order relativistic correction leads to the spectrum shown as *dashed line*. Plasma parameters are as in Fig. 3

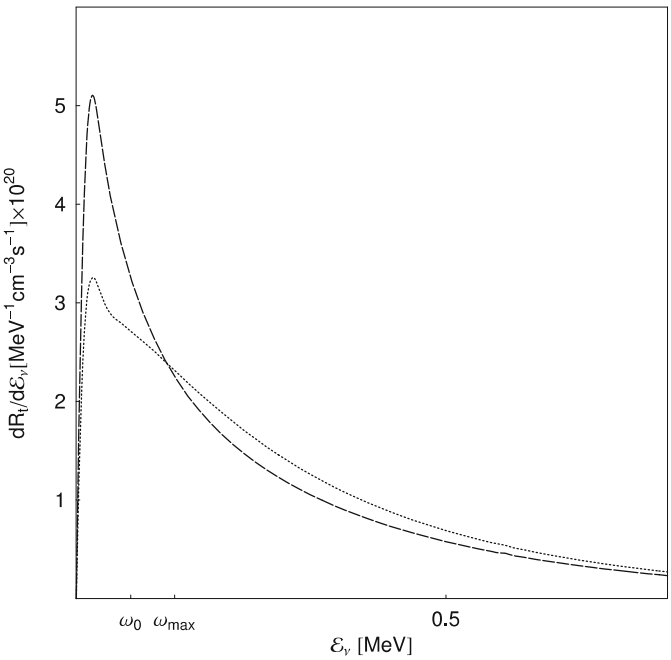


**Fig. 6.** Spectrum of the muon neutrinos (*dotted*) and antineutrinos (*dashed*) from transverse plasmon decay. Contributions to the spectra from the so-called mixed "vector–axial channel" produces significant differences. For electron flavor, the contribution from the "mixed channel" leads to unimportant differences. For both flavors, the contribution from the "axial channel" remains relatively small: $10^{-4}$ for $\nu_e$ and $10^{-2}$ for $\nu_\mu$. The overall contribution to the total emissivity from the $\mu, \tau$ flavors is suppressed relative to electron flavor by a factor $(C_{\rm V}^{\mu,\tau}/C_{\rm V}^{e})^2 \simeq 3.3\times 10^{-3}$

in both the low and high neutrino energy part with the spectrum obtained from the Braaten–Segel approximation for the dispersion relations. The dispersion relation (17a) produces a much larger error, and the spectrum *nowhere* agrees with the correct result. This fact is not a big surprise: as was pointed out by Braaten [16] the dispersion relation is crucial. Therefore, all previous results, including the seminal BPS work [12], could easily be improved just by the trivial replacement $\omega_0 \to m_{\rm t}$. Moreover, the closely related photoneutrino process also has been computed [3, 12, 14, 17] with the simplified dispersion relation (17a) with $\omega_0$. One exception is the work of Esposito et al. [70]. It remains unclear, however, which result is better, as accurate dispersion relations have never been used within a photoneutrino process context. For a plasmaneutrino, (17b) is a much better approximation than (17a), especially if one puts $m_{\rm t}$ from the exact formula (6). The high energy tail of the spectrum also will be exact in this case.

As formula (41) agrees perfectly with the tail of the spectrum, we may use it to derive a very useful analytical expression. Leaving only leading terms of the rational function (42),

$$P(ct,x) \sim x^{-1}(1-ct)^{-2}\,,$$

one is able to compute the integral (41) analytically:

$$\lambda(\mathcal{E}) \simeq \frac{G_{\rm F}^2 C_{\rm V}^2}{64\pi^4\alpha}\frac{m_{\rm t}^6}{\hbar^3 c^9}\left[\kappa - \frac{2}{a}\ln\left(\mathrm{e}^{a\kappa/2}-1\right)\right], \qquad (43)$$

where $\kappa = 2x + (2x)^{-1}$, $x = \mathcal{E}/m_{\rm t}$ and $a = m_{\rm t}/kT$. Interestingly, the spectrum (43) is invariant under the transformation

$$\mathcal{E}'\mathcal{E} = m_{\rm t}^2/4\,,$$

and all results obtained for the high energy tail of the spectrum immediately may be transformed for the low energy approximation. The asymptotic behavior of (43) for $\mathcal{E} \gg kT$ is of main interest:

$$\lambda(\mathcal{E}_\nu) = AkTm_{\rm t}^6 \exp\left(-\frac{\mathcal{E}_\nu}{kT}\right), \qquad (44)$$

where for electron neutrinos

$$A = \frac{G_{\rm F}^2 C_{\rm V}^2}{8\pi^4\alpha}\frac{1}{\hbar^4 c^9} = 2.115\times 10^{30}\,\mathrm{MeV^{-8}cm^{-3}s^{-1}}$$

and $m_{\rm t}$ and $kT$ are in MeV. For the $\mu,\tau$ neutrinos just replace $A$ with $A(C_{\rm V}^{\mu,\tau}/C_{\rm V}^{e})^2$.

Formula (44) gives also quite reasonable estimates of the total emissivity $Q_{\rm t}$ and the mean neutrino energies $\langle\mathcal{E}_\nu\rangle$:

$$Q_{\rm t} = AkT^3m_{\rm t}^6 \qquad (45a)$$

$$\langle\mathcal{E}_\nu\rangle = kT\,. \qquad (45b)$$

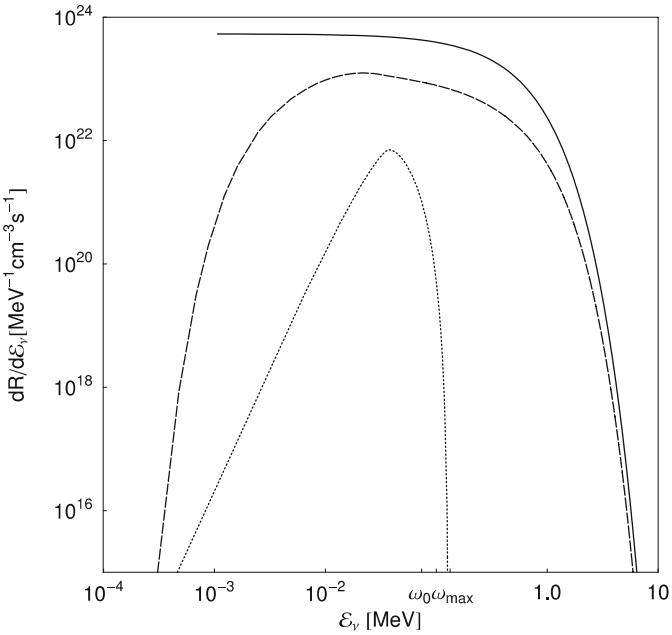


**Fig. 7.** Typical spectra from the plasma process. *Dotted line* is a longitudinal and *dashed* transverse spectrum. Only the $\sim\exp(-\mathcal{E}_\nu/kT)$ tail of the transverse spectrum (*solid line*) contributes to a (possibly) detectable signal. Plasma properties are according to Table 1

For comparison, we mention that Braaten–Segel [15] derived the exact formulae in the high temperature limit $kT \gg \omega_0$:

$$Q_{\rm t}^{\rm BS} = \frac{G_{\rm F}^2 C_{\rm V}^2 \zeta(3)}{12\pi^4\alpha}kT^3m_{\rm t}^6 = 0.8AkT^3m_{\rm t}^6\,, \qquad (46a)$$

$$\langle\mathcal{E}_\nu^{\rm BS}\rangle = \frac{6\zeta(3)}{\pi^2}kT = 0.73kT\,. \qquad (46b)$$

The formulae above agree with $\sim 25\%$ error in the leading coefficients.

### 2.4.2 Numerical results

The calculation of the spectrum in the framework of the Braaten–Segel approximation requires a residue factor, the polarization function [15] (transverse and axial) and the Jacobian [65]:

$$Z_{\rm t}^{\rm BS} = \frac{2\omega_{\rm t}^2\left(\omega_{\rm t}^2 - v_*^2k^2\right)}{3\omega_0^2\omega_{\rm t}^2 + \left(\omega_{\rm t}^2+k^2\right)\left(\omega_{\rm t}^2 - v_*^2k^2\right) - 2\omega_{\rm t}^2\left(\omega_{\rm t}^2-k^2\right)}\,, \qquad (47)$$

$$\Pi_{\rm t}^{\rm BS} = \frac{3\omega_0^2}{2v_*^2}\left(\frac{\omega_{\rm t}^2}{k^2} - \frac{\omega_{\rm t}^2 - v_*^2k^2}{k^2}\frac{\omega_{\rm t}}{2v_*k}\ln\frac{\omega_{\rm t}+v_*k}{\omega_{\rm t}-v_*k}\right), \qquad (48)$$

$$\Pi_{\rm A}^{\rm BS} = \omega_{\rm A}k\frac{\omega_{\rm t}^2-k^2}{\omega_{\rm t}^2-v_*^2k^2}\frac{3\omega_0^2 - 2(\omega_{\rm t}^2-k^2)}{\omega_0^2}\,, \qquad (49)$$

$$J_{\rm t}^{\rm BS} = \frac{\mathcal{E}_1+\mathcal{E}_2}{\mathcal{E}_1\mathcal{E}_2}\left|\frac{1-\beta_{\rm t}^{\rm BS}}{1-\frac{\omega_{\rm t}^2}{k^2}\beta_{\rm t}^{\rm BS}}\right|, \qquad (50)$$

$$\beta_{\rm t}^{\rm BS} = \frac{9\omega_0^2}{4v_*^2k^2}\left[1+\frac{1}{6}\left(\frac{v_*k}{\omega_{\rm t}} - \frac{3\omega_{\rm t}}{v_*k}\right)\ln\frac{\omega_{\rm t}+v_*k}{\omega_{\rm t}-v_*k}\right]. \qquad (51)$$

As an example, a spectrum computed as an integral of (31) over $\mathrm{d}\mathcal{E}_2$ is shown in Fig. 5.

## 3 Summary

The main new results presented in the article are analytical formulae for the neutrino spectra (36) and (41) and the exact analytical formula (44) for the high energy tail of the transverse spectrum. The latter is of main interest from the point of view of detection of astrophysical sources; recently available detection techniques are unable to detect keV plasmaneutrinos emitted with typical energies $\langle\mathcal{E}_\nu\rangle \sim \omega_0/2$ (Figs. 4 and 6), where $\omega_0$ is the plasma frequency (2). The tail behavior of the transverse spectrum quickly "decouples" from the $\omega_0$ dominated maximum area and becomes dominated by the temperature-dependent term $\exp(-\mathcal{E}_\nu/kT)$. Calculation of the events in the detector is then straightforward, as the detector threshold in the realistic experiment will be above maximum area. This approach is much more reliable than the typical practice, where an average neutrino energy is used as a parameter in an arbitrary analytical formula.

Analytical formulae for the spectrum are shown to be a poor approximation of the realistic situation, especially for longitudinal plasmons (see Fig. 4). This is in the agreement with general remarks on the dispersion relations presented by Braaten [16]. On the contrary, the Braaten and Segel [15] approximation is shown to be a very good approach not only for the total emissivities, but also for the spectrum. An exception is the tail of the massive photon decay neutrino spectrum: the Braaten and Segel [15] formulae lead one to underestimate the thermal photon mass, while (44) gives an exact result. The numerical difference between $m_{\mathrm{t}}$ from (6) and (21) is however small [15]. Calculating of the emissivities by the spectrum integration seems a much longer route compared to typical methods, but we are given much more insight into details of the process. For example, we obtain exact formulae for the tail for free this way. An interesting surprise revealed in the course of our calculations is the importance of the high-momentum behavior of the massive photon. While mathematically identical to the simplest approach used in the early calculations, (17b) gives a much better approximation for the total emissivity than (17a).

*Acknowledgements.* This work was supported by a grant of the Polish Ministry of Education and Science (former Ministry of Scientific Research and Information Technology, now Ministry of Science and Higher Education), No. 1 P03D 005 28.

## References

1. D. Arnett, Supernovae and Nucleosynthesis (Princeton University Press, Princeton, 1996)
2. G.S. Bisnovatyi-Kogan, Stellar Physics. Vol. 1: Fundamental Concepts and Stellar Equilibrium (Springer, Berlin, 2001)
3. H. Munakata, Y. Kohyama, N. Itoh, Astrophys. J. **296**, 197 (1985)
4. H. Munakata, Y. Kohyama, N. Itoh, Astrophys. J. **304**, 580 (1986)
5. Y. Kohyama, N. Itoh, H. Munakata, Astrophys. J. **310**, 815 (1986)
6. N. Itoh, T. Adachi, M. Nakagawa, Y. Kohyama, H. Munakata, Astrophys. J. **339**, 354 (1989)
7. N. Itoh, T. Adachi, M. Nakagawa, Y. Kohyama, H. Munakata, Astrophys. J. **360**, 741 (1990)
8. N. Itoh, H. Mutoh, A. Hikita, Y. Kohyama, Astrophys. J. **395**, 622 (1992)
9. Y. Kohyama, N. Itoh, A. Obama, H. Mutoh, Astrophys. J. **415**, 267 (1993)
10. Y. Kohyama, N. Itoh, A. Obama, H. Hayashi, Astrophys. J. **431**, 761 (1994)
11. N. Itoh, H. Hayashi, A. Nishikawa, Y. Kohyama, Astrophys. J. **102**, 411 (1996)
12. G. Beaudet, V. Petrosian, E.E. Salpeter, Astrophys. J. **150**, 979 (1967)
13. J.B. Adams, M.A. Ruderman, C.H. Woo, Phys. Rev. **129**, 1383 (1963)
14. D.A. Dicus, Phys. Rev. D **6**, 941 (1972)
15. E. Braaten, D. Segel, Phys. Rev. D **48**, 1478 (1993)
16. E. Braaten, Phys. Rev. Lett. **66**, 1655 (1991)
17. P.J. Schinder, D.N. Schramm, P.J. Wiita, S.H. Margolis, D.L. Tubbs, Astrophys. J. **313**, 531 (1987)
18. S.I. Blinnikov, M.A. Rudzskij, Astron. Zh. **66**, 730 (1989)
19. S.I. Blinnikov, M.A. Rudzskii, Sov. Astron. **33**, 377 (1989)
20. M. Haft, G. Raffelt, A. Weiss, Astrophys. J. **425**, 222 (1994)
21. F. Reines, C.L. Cowan, Phys. Rev. **113**, 273 (1959)
22. http://www-sk.icrr.u-tokyo.ac.jp/sk/index-e.html
23. J.F. Beacom, M.R. Vagins, Phys. Rev. Lett. **93**, 171 101 (2004)
24. J.F. Beacom, L.E. Strigari, Phys. Rev. C **73**, 035 807 (2006)
25. M. Wurm et. al., Phys. Rev. D **75**, 023 007 (2007)
26. http://sn1987a-20th.physics.uci.edu/
27. G.L. Fogli, E. Lisi, A. Mirizzi, D. Montanino, JCAP **0504**, 002 (2005)
28. http://neutrino.phys.washington.edu/nnn06/
29. J.G. Learned, S.T. Dye, S. Pakvasa, Neutrino Geophysics Conference Introduction, Earth, Moon, and Planets **99**, 1 (2006)
30. http://www.phys.hawaii.edu/ sdye/hano.html
31. J.G. Learned, White paper on Gigaton Array, www.phys.hawaii.edu/∼jgl/post/gigaton_array.pdf
32. R. Davis Jr., Phys. Rev. Lett. **12**, 303 (1964)
33. J.N. Bahcall, R. Davis Jr., Science **191**, 264 (1976)
34. GALLEX-Collaboration, P. Anselmann et al., Phys. Lett. B **357**, 237 (1995)
35. W. Hampel et al., Phys. Lett. B **388**, 384 (1996)
36. N. Bahcall, B.T. Cleveland, R. Davis et al., Phys. Rev. Lett. **40**, 1351 (1978)
37. SNO Collaboration, Q.R. Ahmad, Phys. Rev. Lett. **87**, 071 301 (2001)
38. S. Hirata et al., Phys. Rev. Lett. **65**, 1297 (1990)
39. S. Hirata et al., Phys. Rev. Lett. **66**, 9 (1991)
40. S. Hirata et al., Phys. Rev. D **44**, 2241 (1991)
41. K.S. Hirata et al., Phys. Rev. D **38**, 448 (1988)
42. K.S. Hirata et al., Phys. Rev. Lett. **58**, 1490 (1987)
43. IMB, R.M. Bionta et al., Phys. Rev. Lett. **58**, 1494 (1987)
44. P. Galeotti et al., Helv. Phys. Acta **60**, 619 (1987)
45. E.N. Alekseev, L.N. Alekseeva, V.I. Volchenko, I.V. Krivosheina, JETP Lett. **45**, 589 (1987)
46. E.N. Alekseev, L.N. Alekseeva, V.I. Volchenko, I.V. Krivosheina, Pisma. Zh. Eksp. Teor. Fiz. **45**, 461 (1987)
47. A.E. Chudakov, Y.S. Elensky, S.P. Mikheev, JETP Lett. **46**, 373 (1987)
48. A.E. Chudakov, Y.S. Elensky, S.P. Mikheev, Pisma. Zh. Eksp. Teor. Fiz. **46**, 297 (1987)
49. E.N. Alekseev, L.N. Alekseeva, I.V. Krivosheina, V.I. Volchenko, Phys. Lett. B **205**, 209 (1988)
50. J.N. Bahcall, M.H. Pinsonneault, Rev. Mod. Phys. **64**, 885 (1992)
51. J.N. Bahcall, R.N. Ulrich, Rev. Mod. Phys. **60**, 297 (1988)
52. S. Turck-Chieze, I. Lopes, Astrophys. J. **408**, 347 (1993)
53. H.-Th. Janka, K. Langanke, A. Marek, G. Martinez-Pinedo, B. Muller, Theory of core-collapse supernovae, Physics Reports, Vol. 442, Issues 1–6, The Hans Bethe Centennial Volume 1906–2006, April 2007, p. 38–74
54. A. Burrows, Nature **403**, 727 (2000)

55. J. Blondin, A. Mezzacappa, Nature **445**, 58 (2007)
56. K. Kotake, S. Yamada, K. Sato, Phys. Rev. D **68**, 044 023 (2003)
57. H.A. Bethe, Rev. Mod. Phys. **62**, 801 (1990)
58. J.A. Pons, A.W. Steiner, M. Prakash, J.M. Lattimer, Phys. Rev. Lett. **86**, 5223 (2001)
59. G. Raffelt, A. Weiss, Astron. Astrophys. **264**, 536 (1992)
60. L.G. Althaus, E. Garcia-Berro, J. Isern, A.H. Corsico, Astron. Astrophys. **441**, 689 (2005)
61. W. Hillebrandt, J.C. Niemeyer, Ann. Rev. Astron. Astrophys. **38**, 191 (2000)
62. D.G. Yakovlev, A.D. Kaminker, O.Y. Gnedin, P. Haensel, Phys. Rep. **354**, 1 (2001)
63. S.E. Woosley, A. Heger, T.A. Weaver, RMP **74**, 1015 (2002)
64. BOREXINO Collaboration, S. Schönert et al., physics/0408032 [Nucl. Instrum. Method. A (to be published)]
65. S. Ratković, S.I. Dutta, M. Prakash, Phys. Rev. D **67**, 123 002 (2003)
66. S.I. Dutta, S. Ratković, M. Prakash, Phys. Rev. D **69**, 023 005 (2004)
67. M. Misiaszek, A. Odrzywoltek, M. Kutschera, Phys. Rev. D **74**, 043 006 (2006)
68. W.M. Yao, C. Amsler, D. Asner, R. Barnett, J. Beringer, P. Burchat, C. Carone, C. Caso, O. Dahl, G. D'Ambrosio et al., J. Phys. G **33**, 1 (2006) http://pdg.lbl.gov
69. N. Itoh, A. Nishikawa, Y. Kohyama, Astrophys. J. **470**, 1015 (1996)
70. S. Esposito, G. Mangano, G. Miele, I. Picardi, O. Pisanti, Nucl. Phys. B **658**, 217 (2003)